ACS APPLIED MATERIALS & INTERFACES

Research Article

www.acsami.org

Influence of the Polymeric Interphase Design on the Interfacial Properties of (Fiber-Reinforced) Composites

Christian Kuttner,[†] Andreas Hanisch,[‡] Holger Schmalz,[‡] Michaela Eder,[§] Helmut Schlaad,[⊥] Ingo Burgert,[§,#,∥] and Andreas Fery*[,†]

[†]Department of Physical Chemistry II and [‡]Macromolecular Chemistry II, University of Bayreuth, Bayreuth 95440, Germany

[§]Department of Biomaterials and [⊥]Department of Colloid Chemistry, Max Planck Institute of Colloids and Interfaces, Potsdam 14424, Germany

[#]ETH Zurich, Institute of Building Materials, Zurich 8093, Switzerland

[∥]Empa - Swiss Federal Laboratories for Material Testing and Research, Applied Wood Research Laboratory, 8600 Dübendorf, Switzerland

Supporting Information

ABSTRACT: In fiber-reinforced composites, the interphase nanostructure (i.e., the extended region between two phases in contact) has a pronounced influence on their interfacial adhesion. This work aims at establishing a link between the interphase design of PS-based polymeric fiber coatings and their influence on the micromechanical performance of epoxy-based composite materials. Thiol−ene photochemistry was utilized to introduce a polymeric gradient on silica-like surfaces following a two-step approach without additional photoinitiator. Two complementary grafting-techniques were adapted to modify glass fibers: "Grafting-onto" deposition of PB-*b*-PS diblock copolymers for thin-film coatings (thickness <20 nm) at low grafting density (<0.1 chains/nm^2) - and "grafting-from" polymerization for brush-like PS homopolymer coatings of higher thickness (up to 225 nm) and higher density. Polymer-coated glass fibers were characterized for polymer content using thermogravimetric analysis (TGA) and their nanostructural morphologies by scanning electron microscopy (SEM). Model substrates of flat glass and silicon were studied by atomic force microscopy (AFM) and spectroscopic ellipsometry (SE). The change in interfacial shear strength (IFSS) due to fiber modification was determined by a single fiber pull-out experiment. Thick coatings (>40 nm) resulted in a 50% decrease in IFSS. Higher shear strength occurred for thinner coatings of homopolymer and for lower grafting densities of copolymer. Increased IFSS (10%) was found upon dilution of the surface chain density by mixing copolymers. We show that the interfacial shear strength can be increased by tailoring of the interphase design, even for systems with inherently poor adhesion. Perspectives of polymeric fiber coatings for tailored matrix−fiber compatibility and interfacial adhesion are discussed.

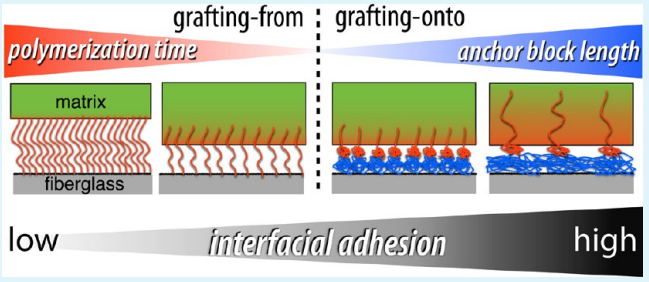

KEYWORDS: *thiol−ene photochemistry, polymer grafting, fiber coatings, composite interphase, micromechanics, interfacial adhesion*

1. INTRODUCTION

Engineered composite materials have become an important foundation of many of todays' technologies and structures. Of these, fiberglass-reinforced composites in particular have found applications in fields like the automotive and aerospace industries, which demand lightweight materials with a high rigidity and strength.[1,2] To satisfy the various technological demands, an adjusted and sufficient interfacial adhesion between fibers and resinous matrix is of crucial importance.[3] Adhesion largely depends on molecular interfacial structures and molecular interfacial interactions.[4] Hence, fiber surface modification by coatings has been identified as a suitable way to influence and control the adhesion and compatibility of the constituent materials.[5,6] Low-molecular-weight modifications are common practice (e.g., by silylation),[6] whereas polymeric modifications are often avoided because of higher costs and elaborate procedures. Additionally, many applied polymers inherently exhibit poor adhesion due to a lack of polar functional groups and a low surface free energy.[7]

Many biological materials are composites, with examples ranging from the mineral protein composites of bone to the polymer−polymer composites making up the plant cell wall. Despite the constituent materials often having poor properties, Nature manages to produce bulk materials with excellent properties that arise through exquisite control of interfaces between the constituents.[8,9] It is hoped that a fundamental understanding of interfacial design in nature will give rise to new ideas for future applications.

Received: November 13, 2012
Accepted: February 27, 2013
Published: February 27, 2013

 © 2013 American Chemical Society

The surface morphology influences the compatibility of coatings and the resulting compound stability.[10] The presence of an interphase[11] with a molecular gradient (an extended region, where two adjacent components are mixed) can promote adhesion and compatibility at the composite interface.[12] To further improve and develop advanced composite materials, a solid understanding of interface/interphase concepts is essential. The influence of different low-molecular-weight modifications (e.g., silanes)[13−15] and macromolecular modifications[16−19] on interphase systems has been studied to enhance bond performance.

In this paper, we deal with the nanostructural aspects of interphase design, by preparing interphase structures by polymer grafting.[20] To understand the effect of nanoscale modifications on the micromechanical performance, we systematically varied surface chain density and chain length of tethered polymer chains in order to achieve various adjusted morphologies.

We applied UV-initiated thiol−ene photochemistry (without additional photoinitiator) to generate surfaces of tethered polystyrene chains on fiberglass. Surfaces are first sulfhydrylated and then modified with polystyrene (PS) upon irradiation of UVA-light. Both "grafting-onto" and "grafting-from" were used as complementary techniques to obtain a broad range of grafting densities. "Grafting-onto" of preformed copolymers (PB-*b*-PS) is a robust technique for thin-film coatings (<20 nm) of low surface chain densities (<0.1 chains/nm^2). For coatings with higher grafting densities, we applied "grafting-from" photopolymerization. The thickness of the coating was controlled by the duration of the light exposure (up to 225 nm within 48 h). The resulting morphologies were characterized and compared to flat glass slides as model substrates. Modified glass fibers, embedded in a microdroplet of epoxy resin, were used for single fiber pull-out tests to measure the interfacial shear strength of the composite interface.[21,22]

Finally, we discuss the interfacial adhesion in composites based on a correlation of the macromolecular interphase nanostructure and the micromechanical performance.

2. EXPERIMENTAL SECTION

2.1. Materials and Reagents. Substrates: fiberglass 365 S-2 rovings, with a filament thickness of 9 μm (AGY-Europe, France); (100)-oriented single-crystal boron-doped silicon (CrysTec, Germany); glass slides of standard soda-lime glass (Menzel-Gläser, Thermo Scientific, Germany). Chemicals were purchased from Sigma-Aldrich unless mentioned differently: styrene (99.9%), purified from stabilizers by filtration through basic alumina column; polybutadiene (PB, approximately 62 mol.% of 1,2-addition). For sulfhydrylation (3-mercaptopropyl) trimethoxysilane (MPTMS, 95%) was used. Solvents, used as received: *n*-heptane (99%, Roth), isopropyl alcohol (99.7%), dichloromethane (DCM, 99.8%), toluene (99.8%), unstabilized tetrahydrofuran (THF, 99.9%, Roth), and cyclohexane (99.5%). Further reagents: ammonium hydroxide (25%, Fluka), hydrogen peroxide (30%, VWR). Deionized water (DI) was obtained from a water purification system (Milli-Q Advantage A10, Millipore). The cold-curing epoxy resin was purchased from R&G Composite Technology GmbH, Germany: epoxy resin L (bisphenol A/F-epichlorhydrin resin) and curing agent S (Mannich base of *p-tert*-butyl-phenol and diamines) mixed in 10:4 ratio. For anionic polymerization of the polybutadiene-*block*-polystyrene (PB-*b*-PS) diblock copolymers, monomers and solvents had to be purified thoroughly before use. THF was freshly distilled from CaH_2 and K metal under dry nitrogen. 1,3-Butadiene (2.5, Rießner-Gase) was passed through columns filled with molecular sieves (4 Å) and basic aluminum oxide and then stored over Bu_2Mg. Styrene (BASF) was degassed three times via freeze/pump/thaw cycles. Afterward, it was stirred over Bu_2Mg and condensed under high vacuum into storage ampules and kept under N_2 until use. *sec*-Butyllithium (*sec*-BuLi, 1.3 M in cyclohexane:hexane, 92:8, Acros) and Bu_2Mg (1 M in heptane) were used as received.

2.2. Block Copolymer Synthesis. The different PB-*b*-PS diblock copolymers were synthesized via anionic polymerization in THF at low temperatures in the presence of alkoxides according to standard procedures.[23] By using THF as polar solvent, butadiene addition preferentially took place in a 1,2 fashion. A thermostatically controlled laboratory autoclave was used, which was equipped with an outlet tube, allowing sampling during polymerization. The polymerization of styrene was started at −70 °C using *sec*-BuLi as initiator. After 30 min butadiene was added at −70 °C and then polymerized at −20 °C to −15 °C. At the desired conversion − as followed by in-line near-infrared fiber-optic spectroscopy − samples were withdrawn and precipitated into degassed isopropyl alcohol after polymerization times ranging from 30 min to 24 h. This allowed a series of polymers with the same polystyrene block, but different degrees of polymerization of the polybutadiene block to be synthesized.

2.3. General Procedure of the Two-Step Polymer Grafting. *Cleaning and Sulfhydrylation.* Fiberglass was ultrasonically cleaned for 15 min in an aqueous solution of isopropyl alcohol (75 vol.%), rinsed with DI water and immersed in a mixture of DI water, hydrogen peroxide and ammonium hydroxide (5:1:1 by volume) at 70 °C for 10 min to remove organic residues (e.g., fiberglass sizing) and to complete hydroxylation.[24] Activated fiberglass was removed from solution and thoroughly rinsed with DI water. To minimize the amount of water available for hydrolysis of MPTMS, substrates were successively cleaned with *n*-heptane, THF, and cyclohexane upon ultrasonication (15 min each). Direct sulfhydrylation of the activated surfaces was performed by immersion in a MPTMS solution of 0.1 vol. % in *n*-heptane (5.5 mM, Ar atmosphere, 24 h at RT), followed by a sequential washing upon ultrasonication (*n*-heptane, DCM, toluene, cyclohexane, and THF for 10 min each) to remove physisorbed species.

Photochemical Polymer Grafting. MPTMS-modified fiberglass was directly transferred to either a 34 mol.% solution of styrene monomer in cyclohexane ("grafting-from" method), or to a 2.1 wt.% solution of PB-*b*-PS diblock copolymer in cyclohexane ("grafting-onto" method) under Ar atmosphere. Polymerization was carried out upon irradiation with UV/visible light (Höhnle UV F 400F, 400 W, blue filter: 320 nm < λ < 420 nm) for 24 h for "grafting-onto" and for different durations (3, 6, 12, 24, 36, and 48 h) for "grafting-from". The temperature was kept below 30 °C. Polymer-grafted substrates were sequentially washed upon ultra sonication (THF, DCM, toluene, cyclohexane, and DI water for 10 min each) and dried overnight at 30 °C.

2.4. Surface Characterization Methods. The fiberglass surface was imaged by scanning electron microscopy (SEM) (Leo1530, Zeiss). Flat substrates (silicon wafers) were investigated by atomic force microscopy (AFM) in tapping mode (Dimension V, Veeco Metrology Group, USA) with AC160TS-W2 cantilevers (300 kHz, 42 N/m) by Olympus. The thickness of thin films on fiberglass was calculated from thermogravimetric analysis (TGA) (N_2 flow, heating rate of 5 °C/min, TGA/SDTA 851e, Mettler Toledo). The film thickness on flat substrates was evaluated by AFM scratch analysis and spectroscopic ellipsometry (SE) with PSCA configuration (SE850, Sentech).

2.5. Micromechanical Characterization. The effect of the modifications on the mechanical properties of the glass-epoxy interface, single glass fiber in epoxy matrix pull-out tests were performed with a custom built setup, based on the method described by Miller et al.[22] A 40−70 μm sized droplet of epoxy was placed on an isolated fiber. After curing (48 h at 60 °C) the fiber end with the epoxy droplet was placed between two metal plates. The distance between the plates was kept small enough to avoid slipping of the droplet. The other end of the fiber was fixed on the load cell (max. capacity 5 N), which is located on the motor controlled, movable part of the tester. The fibers were pulled out of the epoxy droplet at 1 μm/s while simultaneously recording the applied forces. The interfacial shear

strength τ_{max} (abbrev. IFSS) was calculated using the following equation

$$\tau_{max} = \frac{F_{max}}{\pi d l} \quad (1)$$

where F_{max} is the maximum recorded force, d is the glass fiber diameter, and l the length of the droplet along the fiber. A minimum of 5 successful measurements per treatment were performed for those coated using the "grafting-from" method and 8 per treatment for the "grafting-onto" method.

2.6. Diblock Copolymer Characterization. Size-exclusion chromatography (SEC) measurements were performed on a set of 30 cm SDV-gel columns of 5 μm particle size having a pore size of 10^5, 10^4, 10^3, and 10^2 Å with refractive index and UV detection (λ = 254 nm). THF was used as eluent at a flow rate of 1 mL/min using toluene as internal standard. The system was calibrated with polystyrene standards. ^{1}H NMR spectra were recorded at 300 MHz (Ultrashield 300, Bruker) with $CDCl_3$ as solvent and tetramethylsilane as internal standard.

3. RESULTS AND DISCUSSION

3.1. Diblock Copolymer Characterization. To cover the regime of low grafting densities (<0.1 chains/nm^2), we decided to use diblock copolymers with specific block functions for the "grafting-onto" approach. Utilizing a laboratory autoclave system, we synthesized three different series of polybutadiene-*block*-polystyrene (PB-*b*-PS) diblock copolymers (indexed 1 for PB_x-*b*-PS_{78}, 2 for PB_x-*b*-PS_{360}, and 3 for PB_x-*b*-PS_{959}, the subscripts denote the corresponding number-average degree of polymerization) with the same degree of polymerization of polystyrene (PS) but varying polybutadiene (PB) block lengths (SEC, Figure S1 in the Supporting Information).[23] This approach offers the possibility of screening the influence of the ratio of anchor block (PB) to buoy block (PS). Figure 1 shows an overview of block lengths of the applied copolymers.

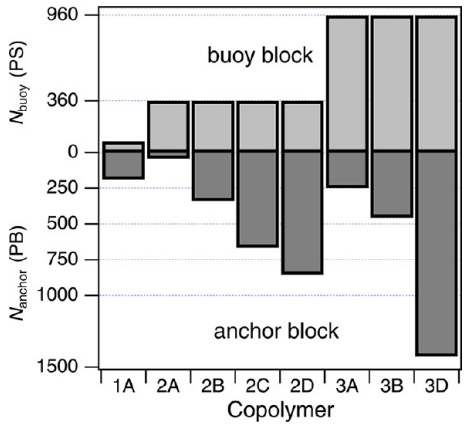

Figure 1. Series of synthesized diblock copolymers of polystyrene (buoy block) and polybutadiene (anchor block).

As the conjugation of the diblock copolymers to the sulfhydrylated surface proceeds via a radical mechanism, a high content of vinyl groups within the PB block is favorable. Therefore, to obtain PB blocks with a high degree of 1,2-addition, anionic polymerization was conducted in THF.[25] The chemical composition of the obtained diblock copolymers as well as the fraction of 1,2-addition $\chi_{1,2}$ within the PB block was determined by ^{1}H NMR spectroscopy. In combination with the number average molecular weight $\langle M_n \rangle$ of the respective PS precursors, as determined by SEC with PS calibration, the overall molecular weight of the synthesized diblock copolymers was calculated from the ratio of the characteristic signals (see Figure S2 in the Supporting Information). The complete data of molecular characterization of the PB-*b*-PS diblock copolymers is summarized in Table 1 (including a commercial PB, used for comparison).

Table 1. Molecular Properties and Micromechanical Performance of Grafted Copolymer, Sorted by Increasing PS Chain Length

copolymer index		$\langle M_n \rangle$ (kg/mol)	$Đ^a$	$\chi_{1,2}{}^b$ (%)	$\langle \sigma_{PS} \rangle^c$ (a.u.)	$\langle \tau_{max} \rangle^d$ (MPa)
$PB_{1,2}$	PB_{29}	1.54	1.62	62		36.3 ± 6.5
1A	PB_{191}-*b*-PS_{78}	18.40	1.12	86.2	0.223	33.3 ± 2.1
2A	PB_{43}-*b*-PS_{360}	39.80	1.03	86.2	1	32.9 ± 2.1
2B	PB_{339}-*b*-PS_{360}	55.80	1.03	85.0	0.126	36.0 ± 3.6
2C	PB_{663}-*b*-PS_{360}	73.30	1.02	86.6	0.0642	38.9 ± 2.9
2D	PB_{854}-*b*-PS_{360}	83.60	1.02	85.8	0.0499	49.0 ± 4.3
3A	PB_{250}-*b*-PS_{959}	113.40	1.02	86.3	0.170	33.3 ± 2.1
3B	PB_{457}-*b*-PS_{959}	124.60	1.03	83.7	0.0931	31.8 ± 2.2
3D	PB_{1426}-*b*-PS_{959}	176.90	1.03	86.5	0.0299	42.3 ± 4.3

[a]Dispersity, determined from SEC (peak of the diblock copolymer, neglecting the precursor and coupling peaks). [b]Number fraction of 1,2-addition of the PB block as determined by ^{1}H NMR spectroscopy. [c]Normalized relative grafting density calculated from scaling theory[26] and normalized to 2A. [d]Interfacial shear strength: de-bonding of a microdroplet of epoxy resin from a single glass fiber.

3.2. Two-Step Photochemical Polymer Grafting. We used both "grafting-onto" and "grafting-from" to attach PS chains at the surface of fiberglass to screen their morphology and micromechanical performance (interfacial adhesion) with a matrix of epoxy resin.

As a first step, SH groups were introduced on the inorganic surface by treatment with (3-mercaptopropyl) trimethoxysilane (MPTMS) to allow thiol−ene photochemistry.[16,27,28] The generation of radicals at the surface is based on the homolytic cleavage of thiol functional groups upon irradiation with UV light without additional photoinitiator.[29,30] Formed sulfenyl radicals are surface-localized and can serve as polymerization initiators ("grafting-from") or anchoring site for preformed solution-borne polymer ("grafting-onto"). The generation of new radicals proceeds sporadically and continuously as long as irradiation with UV light takes place. Although the total concentration of radicals increases progressively with time, the spatial separation of the randomly distributed active sites keeps the local concentration of radicals low. Figure 2 compares the surface of neat fiberglass before (2a) and after the deposition (2b) of a thin precursor layer of MPTMS, imaged by scanning electron microscopy (SEM).

Upon "grafting-onto", the preformed diblock copolymer was attached to surface-localized radicals via an anchoring block (i.e., PB). Figure 2c shows the surface morphology of grafted PB homopolymer, whereas some areas with defects reveal the underlying fiberglass. The presence of the polymer layer was clearly identified from SEM. An example of a PB-*b*-PS

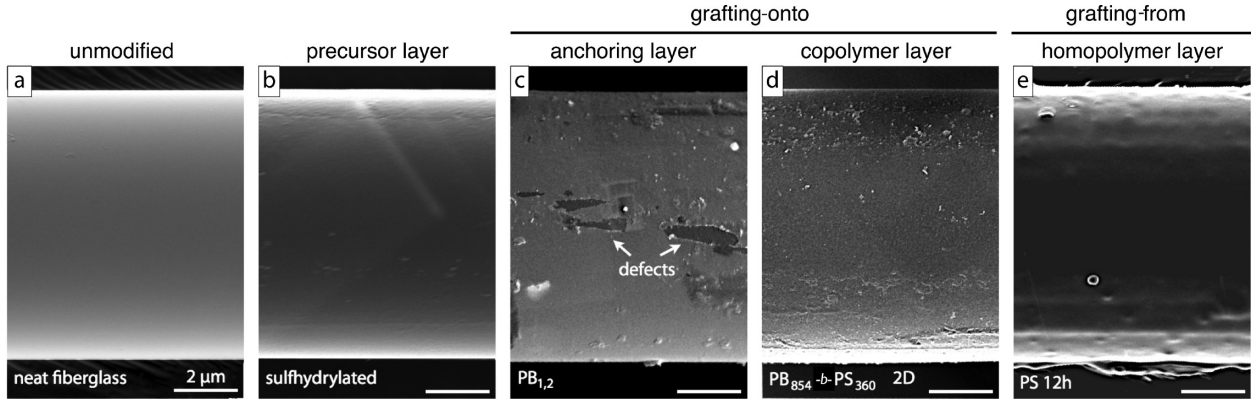

Figure 2. SEM micrographs of fiberglass surfaces: (a) neat fiberglass shows a homogeneous smooth surface structure, which becomes grainier after (b) sulfhydrylation, "grafting-onto" deposition of (c) $PB_{1,2}$, and (d) diblock copolymer PB_{854}-*b*-PS_{360} form grainy layers. In contrast, (e) "grafting-from" polymerization of PS results in thicker (>40 nm, 12 h) brushlike polymer films with a smooth surface.

copolymer grafting is presented in Figure 2d. The grafted polymer forms a thin granular layer (<20 nm) of higher roughness. Since the PB block features many vinyl functions it can be multiply conjugated to the surface and to adjacent polymer chains. Upon deposition, an interpolymer network (IPN) of multiply attached PB chains is formed. All PS blocks are covalently tethered to this IPN.

Because the surface density of the individual PS chains depends on the copolymer length (i.e., volume of polymer coil in solution) and its block ratio, the grafting density, which can be realized by "grafting-onto", is limited. To attain higher grafting densities, "grafting-from" polymerization is the method of choice. The "grafting-from" process is based on the progressive consumption of vinyl monomer to form polymer chains. In the collapsed state, the densely grafted brush-like polymer forms a smooth coating surrounding the fiberglass (Figure 2e). Because polymerization in solution is avoided, all growing chains are attached to the surface. Depending on the time of initiation, the individual polymer chains may exhibit a high dispersity ($Đ \gg 2$). Because the active sites are translocated away from the surface upon chain growth, the chance for termination of newly formed radicals is kept low. This may result in a situation where many active chains, which are densely packed at the surface, can coexist and grow simultaneously. Depending on the polymerization time, different film thicknesses can be obtained (≈100 nm within 24 h), based on a successive increase of both grafting density and mean chain length.[16] Even though the grafting of the polymer is based on a free-radical process, the deposition mechanism proceeds in a controlled manner.

The success of the grafting procedure for covalent attachment of polymer to the fiberglass surface was controlled by thermogravimetric analysis (TGA). Figure 3 shows the relative polymer content by the mass loss of polymer-grafted fiberglass upon progressive heating. From this decomposition, the grafting thickness of the homopolymer attached via "grafting-from", can be calculated.[16] The results for six polymerization times (3, 6, 12, 24, 36, and 48 h) are presented in Table 2 and compared to graftings on flat glass substrates as model systems. Flat substrates allow the thickness determination by common techniques like AFM scratch analysis and spectroscopic ellipsometry (SE), which cannot be applied on fiberglass. Whereas SE gives a mean value of a large area (≈ 20 mm^2), AFM allows very precise local measurements. These results are

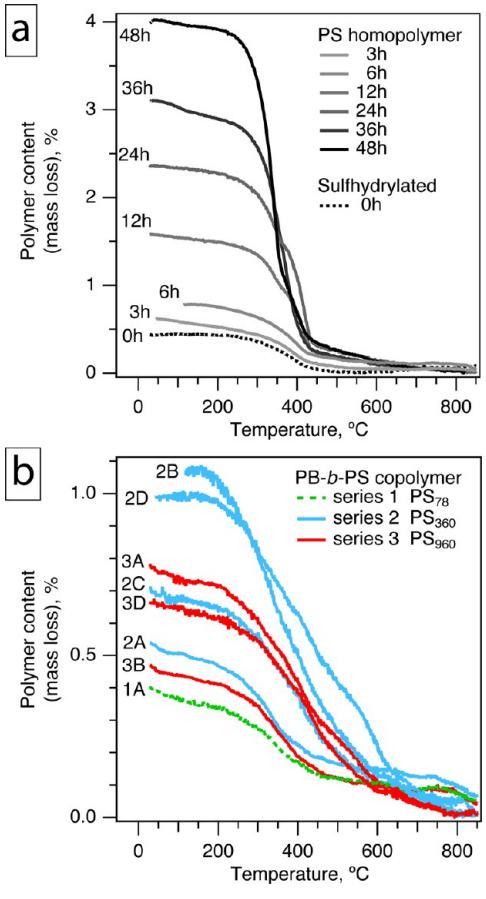

Figure 3. Thermogravimetric analysis of grafted fiberglass showing the polymer content for (a) "grafting-from" and (b) "grafting-onto".

in good agreement, whereas the values calculated from TGA show a high uncertainty.[16]

The calculation of the grafting thickness from TGA data of "grafting-onto" polymerizations fails due to an undefined bulk density of the IPN layer. If the apparent bulk density of the copolymer is applied, the thickness is overestimated and does not coincide with the information from SEM. To study the morphology arising from the "grafting-onto" approach, we prepared graftings on flat model substrates (silicon wafer). Initial SE studies suggested that the grafting does not consist of a closed uniform layer of polymer. To obtain detailed

Table 2. Grafting Thickness and Micromechanical Performance of PS Homopolymer-Grafted Fiberglass and Glass Slides

	grafting thickness in dry state t_{dry} (nm)			
	fiberglass	flat glass substrate		
"grafting-from" polymerization time (h)	TGA[16]	SE	AFM	$\langle\tau_{max}\rangle^a$ (MPa)
3	9 ± 11	8 ± 3	10 ± 3	33.7 ± 1.9
6	18 ± 11	14 ± 3	15 ± 4	27.3 ± 1.7
12	66 ± 18	40 ± 2	43 ± 17	20.8 ± 1.5
24	113 ± 27	95 ± 4	105 ± 7	21.9 ± 1.1
36	144 ± 34	158 ± 3	164 ± 15	21.8 ± 1.9
48	197 ± 45	212 ± 5	225 ± 16	

[a]Interfacial shear strength: de-bonding of a microdroplet of epoxy resin from a single glass fiber.

information about the constitution of the "grafting-onto" layer, we performed AFM, which is the most capable technique to study thin-film topography imageat high spatial resolution.[31−33] Figure 4 shows the morphology of an exemplary graft layer

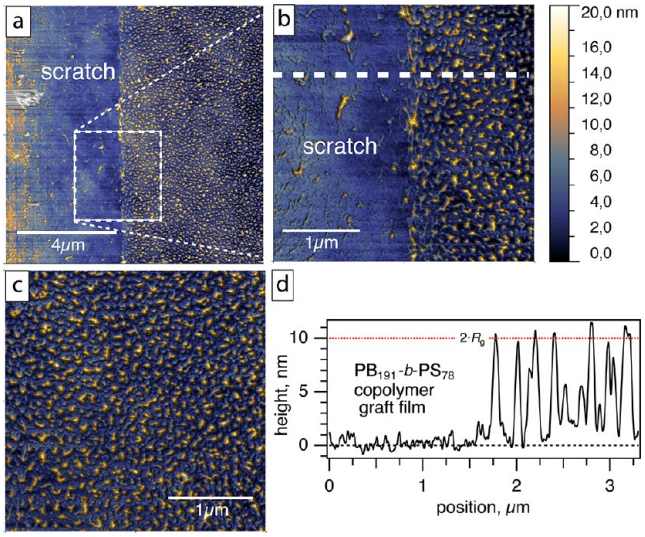

Figure 4. AFM micrographs of a buoy-anchor morphology of an exemplary surface modified with copolymer ("grafting-onto" of PB_{191}-*b*-PS_{78} on flat silicon substrate) in dry state: (a, b) scratched surface layer; (c) the collapsed film consists of copolymer closely packed at the surface; (d) scratch analysis (at dashed line of 4b) shows a height step of 10 nm, which is twice the radius of gyration of the respective copolymer chain ($R_g \approx 5$ nm).

obtained from PB_{191}-*b*-PS_{78}. The morphology of the collapsed copolymer layer shows that the polymer is attached closely packed at the surface. The maximum height of the topography (Figure 4b) corresponds to twice the radius of gyration ($t_{max} \approx 2\ R_g$; see Figure 4d). In this situation in air, the collapsed buoy chains form "blobs" of polymer on top of the closed layer of anchor blocks.[20,26]

The most frequent height of the densely packed buoy-anchor film is in the range of R_g of the copolymer (see Figure 5a). In fact, it is even closer to the R_g of the sole PB block, since here we see the formed interpolymer network (IPN) layer of multiply attached anchor chains. The contribution of the buoy block, which is located on top of the IPN, can be seen in the positive skew of the height distribution. This assumption is supported by the morphology of a PB_{29} homopolymer graft, where we have a discrete IPN layer with a symmetric height distribution (see Figure 5b). As expected, homopolymer layers via "grafting-from" are closed uniform films, where the height distribution is symmetric and represents the surface roughness (see Figure 5c and Figure S3 in the Supporting Information). In the morphology of the homopolymer films, small spherical features can be identified (see Figure 5c), which could be a result of high dispersity of the brush chains. This dispersity is caused by the nature of the photochemical initiation (see above). Due to a low surface roughness of about 1 nm, the grafted layers can still be considered as smooth films.

3.3. Nanostructural Parameters. To correlate the mechanical performance to the interphase structure, the state of the grafted polymer at the surface has to be characterized. We identified the surface chain density (grafting density σ) and the length of the PS chain as the two most characteristic parameters describing the surface nanostructure. The field of tailored grafting densities has been intensively studied because it embodied the foundation for advanced applications like surface gradients,[34−37] responsive coatings,[35,38,39] and anchoring of functional (macro)molecules to the surface.[27,40] Both "grafting-onto"[20,37,41,42] and "grafting-from"[16,20,43−45] approaches have been reported as reliable techniques. Apart from macromolecular anchoring layers,[42] chain attachment or initiation of polymerization is commonly based on a thin precursor film formed by self-assembly (of low molecular weight silanes).[16,44,46]

Our approach is different, since we used thiol−ene photochemistry allowing both "grafting-onto"[27] and "grafting-from".[16] The combination of direct generation of radicals at the surface (without additional photoinitiator) and a low local concentration of reactive sites, allows the free-radical polymerization to proceed in a controlled manner. Chain transfer reactions, especially to solvent and monomer, should be absent to avoid radical polymerization in solution and to ensure that all growing polymer chains are bound to the surface. High grafting efficiency can be obtained by effective suppression of polymerization in solution.[16,29,47] We regard thiol−ene photochemistry as a promising technique for industrial applications.

"Grafting-onto". The morphology of the grafted copolymer film is related to the adsorption of diblock copolymers, where the adsorbed state consists of a swollen anchoring layer and a more diluted and extended buoy layer. Therefore we applied a scaling description for the adsorption from a nonselective solvent (cyclohexane) by Marques and Joanny (MJ).[26] The MJ theory allows for predicting the surface chain density σ of buoy-anchor systems. Depending on the ratio of buoy and anchor block length, the copolymer either falls into a buoy- or anchor-dominated regime. Every copolymer can be described by its anchor fraction ($\nu_{anchor} = N_{anchor}/N$) and its total degree of polymerization N (see Figure 6a). Both regimes exhibit a respective scaling of the grafting density to the copolymer composition. The intersection of the buoy regime scaling (solid line, $\sigma \sim (\nu_{anchor}/(1 - \nu_{anchor}))^{6/5}$) and the anchor regime scaling (dashed line, $\sigma \sim (\nu_{anchor}\ N)^{-1}$) is set at a crossover composition ($N_{buoy} \approx N_{anchor}^{11/6}$). All of our copolymers comply with the anchor regime as shown in Figure 6a ($N_{buoy} < N_{anchor}^{11/6}$). Depending on the total polymerization degree N, the regime crossover is shifted toward lower anchor fractions for increasing length of the copolymer chain.

There is an inverse scaling of the relative grafting density to both the anchor fraction ν_{anchor} and the length of the anchor

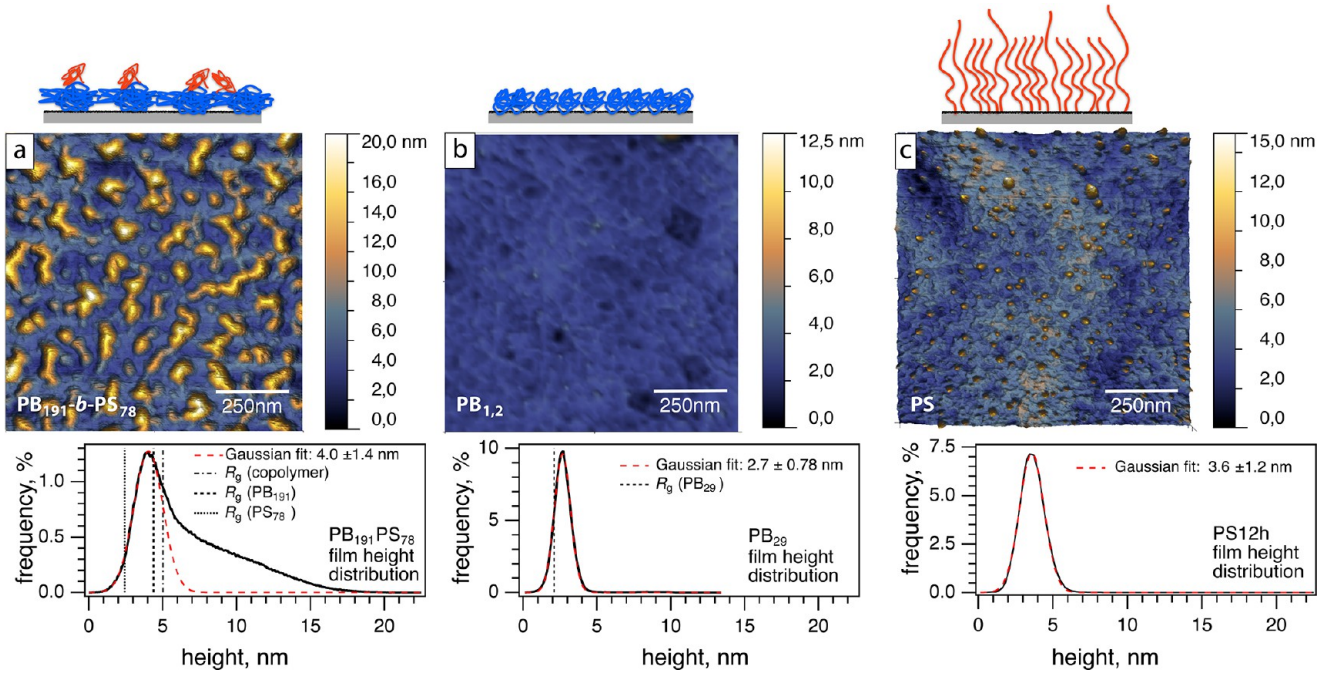

Figure 5. Comparison of surface morphologies on flat silicon substrates imaged by AFM and the corresponding height distributions: (a) PB_{181}-*b*-PS_{78} copolymer, (b) PB_{29} homopolymer, and (c) PS12h homopolymer. On the basis of the skew of the qualitative height distributions, copolymer grafts can be clearly distinguished from homopolymer grafts.

block N_{anchor}. Figure 6b shows the scaling behavior of the relative grafting density for the length of the anchor block by its degree of polymerization (N_{anchor}), normalized to the highest value (2A). The numerical coefficient can be estimated to (0.06 ± 0.02) chains/nm^2 based on the apparent R_g of the anchor block.[23,48] The normalized relative grafting densities are listed in Table 1.

"Grafting-from". It is clear that MJ's theory cannot be applied for the homopolymer films produced by "grafting-from" polymerization. Even though the surface chain density can basically be determined by AFM or TGA,[19,24] a precise determination is not possible for the realized thin films on fiberglass. The main problem is that we neither know the chain length, nor the dispersity of the polymerized brush. Even SEM allows only for rough estimations on this matter. Since the grafting thickness increases linearly with time (see Table 2) it can be expected that both grafting density and chain length increase throughout the grafting process. If the polymerization degree N was known, the grafting density could be calculated from the film thickness. Because the amount of polymer at the surface (e.g., cleaved-off by alkali treatment) is too small, N cannot be directly quantified by size-exclusion chromatography. The common approach of using a sacrificial initiator causing polymerization in solution was not applied since the mechanism of a photoinitiated thiol−ene polymerization is inherently different from classical solution-borne polymerization.

Based on a rough estimation, the maximum achievable chain density is determined by the sterical close packing of polymers yielding 0.9 chains/nm^2 for the case of polystyrene. Especially grafting densities of comparable conditions and molecular weight are found to be higher than 0.1 chains/nm^2, thus we expect a grafting density between 0.1 and 0.9 chains/nm^2.[20,49,50]

Even if the determination of the precise surface chain density is not possible, we can expect that "grafting-from" allows for higher grafting densities ("grafting-onto" < 0.1 chains/nm^2 < "grafting-from"), which is sufficient for a correlation with the micromechanical results. Alternatively, we correlated the micromechanical results to the coating thickness (and the respective polymerization time).

3.4. Mechanical Characterization (Interfacial Shear Strength). Single fiber pull-out tests allowed for determination of the interfacial shear strength τ_{max} (abbrev. IFSS) and discriminating between different fiber surface treatments.[22,51] As a first step, a microdroplet of resin was prepared on the fiber, cured, and mounted in a guillotine-like shearing blade (see Figure S4 in the Supporting Information). When the fiber is pulled, the microdroplet contacts the blades, and will eventually become sheared off. Upon the simplifying assumption, that the debonding force is distributed uniformly on the fiber-matrix interface, the IFSS can be calculated using eq 1. The micromechanical results are included in Tables 1 and 2.

As a final step, we can relate the micromechanical performance to the macromolecular interphase nanostructure. From the "grafting-from" approach, we found a decrease of the interfacial shear strength for thicker grafting films (i.e., longer polymerization times, see Figure 7a). The thickness of the fiberglass coating has a distinct effect on the interfacial stability, the capability to withstand shear stress (Figure 7b). The neat fiberglass showed an IFSS of (42.7 ± 1.9) MPa and outperformed all homopolymer-modified samples. By coating with PS homopolymer, the IFSS gradually decreases until a minimum of ≈21 MPa is reached (12, 24, and 36 h). This might indicate that at a polymerization time of 12 h a maximum grafting density is reached and subsequent film growth is caused by growing and stretching of the active brush chains. Even though we cannot calculate the precise grafting density for the individual polymerization times, we can clearly expect (on

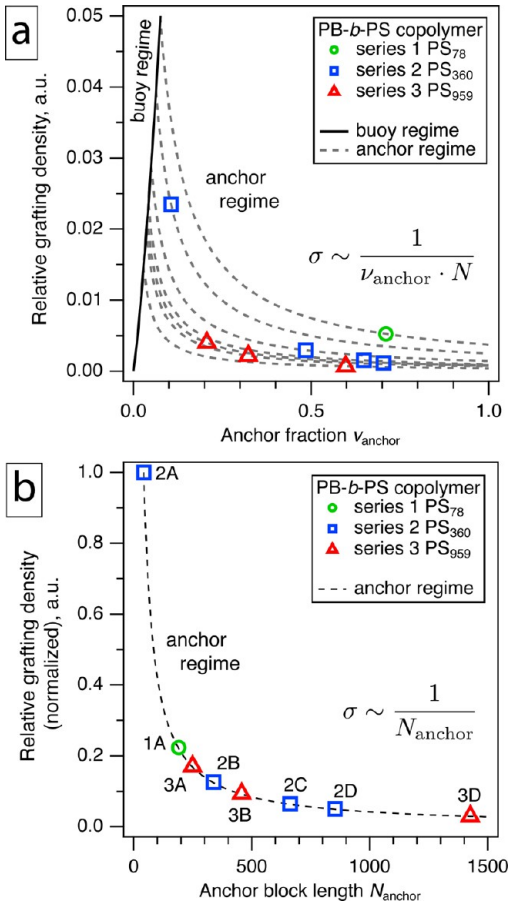

Figure 6. Application of MJ's scaling theory[26] to calculate the relative grafting density of the PS buoy chains from the buoy-anchor copolymer composition: (a) Based on the intersection of buoy regime scaling (solid line) and the anchor regime scaling (dashed line), all applied copolymers comply with the anchor-dominated regime. (b) Normalized relative grafting density scaled for the length of the anchor block by its degree of polymerization.

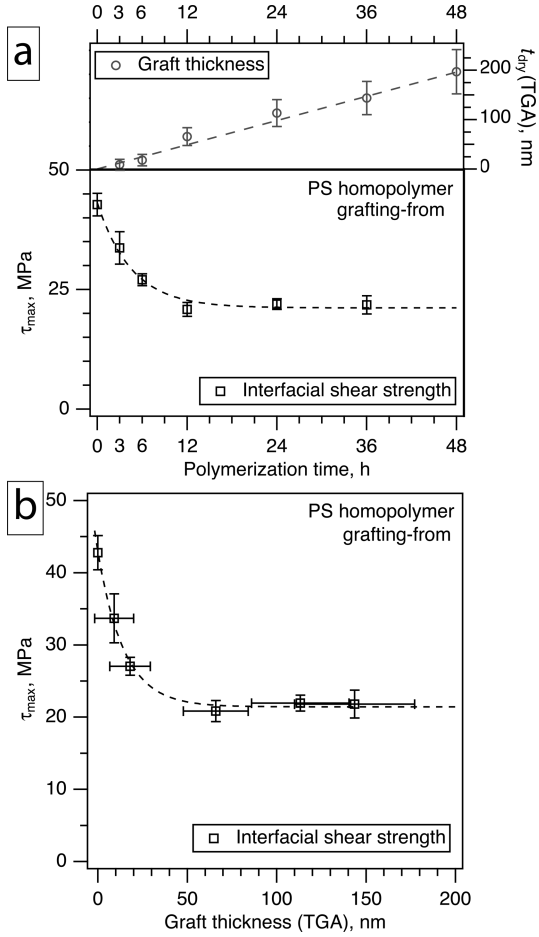

Figure 7. Mechanical performance of PS homopolymer-grafted fiberglass: (a) interfacial shear strength (bottom) and grafting thickness (top) versus polymerization time; (b) interfacial shear strength versus thickness of grafted polymer. The dashed lines are guides to the eye.

the basis of our understanding of the initiation mechanism) that at earlier times, fewer radicals and hence a lower surface coverage of PS chains is realized. For that reason, we expect that the samples of 12, 24, and 36 h are of higher surface density and therefore exhibit the lowest interfacial adhesion.

Figure 8a shows the IFSS of the copolymer-grafted fiberglass. In comparison to neat fiberglass, debonding took place at lower shear forces except for modification 2D and 3D. For series 2 (PB_x-*b*-PS_{360}) a clear trend of higher IFSS for longer anchor chains can be found. Series 3 (PB_x-*b*-PS_{959}) shows a similar dependency in the respect that the copolymer with the longest anchor chain (3D) showed the highest IFSS. The slight deviation (3A, 3B) is within the accuracy of the measurement. The relative surface chain density was calculated from the copolymer composition using MJ's scaling theory (see Section 3.3).[26] Figure 8b presents the correlation of the micromechanical performance and the surface density of the buoy chains (fraction of copolymer that remains free after grafting).

For the "grafting-onto" approach (σ < 0.1 chains/nm^2), we found that samples of lower surface chain density withstood higher shear stress. Copolymer-modifications of higher surface density (1A, 2A, and 3A) yielded low IFSS of ≈33 MPa, close to the result of the homopolymer-modification PS3h (≈34 MPa) of lowest surface density. The highest IFSS were realized by two samples (2D, 3D) with the lowest surface density of the respective series (>42 MPa). The modification 2D (PB_{854}-*b*-PS_{360}) even withstood 49 MPa, which is a 15% increase compared to neat glass fibers.

Additionally, the length of the buoy chains also influenced the IFSS. Modifications of PB_x-*b*-PS_{360} (series 2) resulted in higher IFSS values than the longer PB_x-*b*-PS_{959} (series 3) samples even at higher surface chain densities (2D > 3D and 2B > 3B). This may be due to a better interpenetration of the buoy chains into the resinous matrix.

Overall, it seems that a lower surface chain density leads to increased IFSS and therefore higher interfacial adhesion. To test this theory, we prepared a mixture of 80% PB_{191}-*b*-PS_{78} (1A, short PS chain) and 20% PB_{250}-*b*-PS_{959} (3A, long PS chain), since both have comparable anchor block lengths and IFSS values (≈33 MPa). For the mixture, the effective surface chain density of PS_{959} chains was calculated from eq 2

$$\sigma_{mix} = \frac{1}{4\sigma_{1A}^{-1} + \sigma_{3A}^{-1}} \quad (2)$$

By using shorter chains (<1/10) as spacer molecules, the IFSS was increased by 10% to (36.5 ± 2.5) MPa (see Figure 8).

Further evidence that the grafting density is a most crucial parameter to attain high interfacial adhesion in composite-like

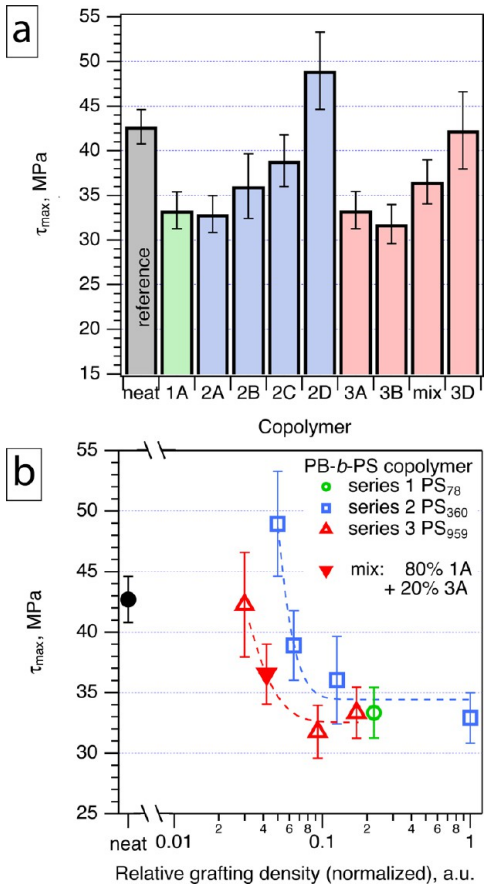

Figure 8. Mechanical performance of PB-*b*-PS diblock copolymer grafted fiberglass: (a) nominal interfacial shear strength; (b) correlation of IFSS to relative grafting density of the buoy chains for three series of copolymers. The term "Mix" denotes a 4:1 mixture of PB_{191}-*b*-PS_{78} (short PS chain) and PB_{250}-*b*-PS_{959} (long PS chain). The dashed lines are guides to the eye.

systems can be found in studies on different fields like wetting autophobicity[52−54] and thin film stabilization.[49] Our findings are in good agreement with Duchet et al. who suggested that the toughness can be improved by the presence of tethered chains at the interface, whereas too high grafting density can sabotage the composite's adhesion.[5]

The applied matrix resin mainly consisted of a bisphenol A-epichlorhydrin (75%), bisphenol-F and hexandioldiglycidyl ether. As curing agent a Mannich base (40%) formed of p-*tert*-butyl-phenol, trimethylhexamethylenediamine, and α,α-diamino-*m*-xylol was used. Upon cold curing (24 h at RT) a strong network was formed based on diglycidyl ethers of bisphenol A. The chemical composition of this network consists of phenyl groups mainly linked by ether functions. Therefore, this uncured epoxy resin network allows the incorporation of polystyrene chains, which results in an enthalpic compatibility. The mechanism of surface-grafted macromolecular connector chains in interphase/interface systems has been intensively studied by Gutowski and co-workers.[55−57] The interpenetrating surface-tethered PS chains can become trapped in the resin network and serve as noncovalent mechanical interlocking agents.

Apart from enthalpic compatibility also entropic contributions have to be considered to achieve high interfacial adhesion. Kim et al. studied chemical thin-film incompatibility and reported that entropic effects play a dominant role in autophobic dewetting.[49] The conventional classification of chemical (i.e., enthalpic) compatibility does not hold for thin-film interfaces and interphase systems. Our finding that nanostructures of higher surface chain density ("grafting-from" approach) are exhibiting lower interfacial adhesion is in agreement with the understanding that entropic effects are of great relevance. Chain penetration into the resinous matrix, or uptake of matrix material by the brushlike film, correlates with a loss in entropy of the stretched chains and a repulsion due to resin network elasticity.[54]

At higher grafting densities ("grafting-from" polymerization), only low IFSS is achieved because of poor miscibility of matrix material and stretched PS chains. The uptake of matrix is poor and both phases remain segregated. Here, the length of the brush chain (i.e., the thickness of the coating) plays an insignificant role and does not allow further stabilization of the fiber-matrix interface. Upon decrease of the grafting density, the incorporation of matrix material into the polymer film is enhanced and a coating-matrix interphase is formed. As a result, the composition becomes able to withstand higher shear stress and exhibits higher IFSS. The grafting density, the local space between tethered chains, is a prerequisite for effective intermixing with matrix material. Coatings of intermediate grafting density are accessible both by "grafting-from" and

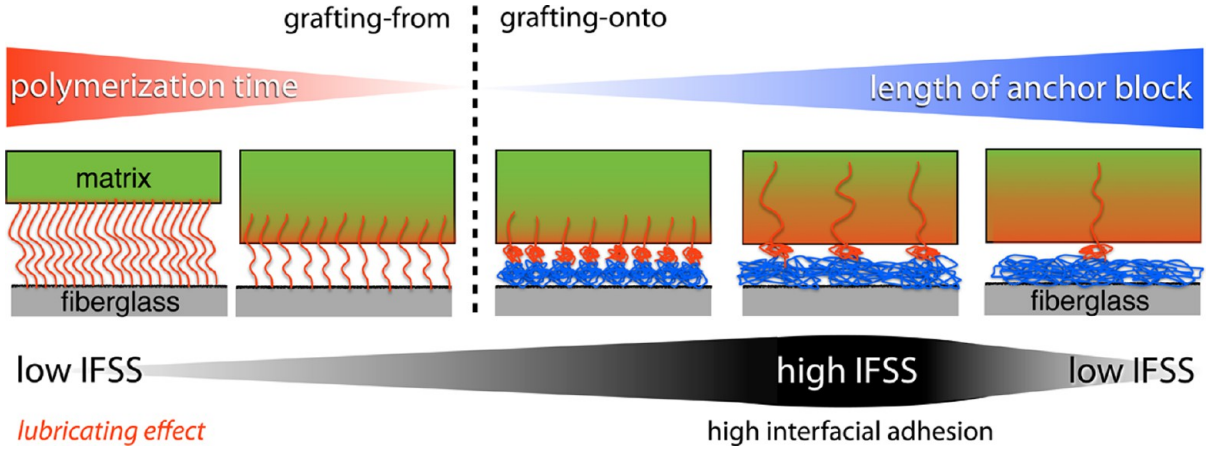

Figure 9. Schematic representation of the interaction of matrix material with grafted polystyrene chains at the surface.

"grafting-onto" techniques. Upon further decreasing the grafting density, a regime of high interfacial adhesion can be found. Here, one has to consider that the grafting density is not the only parameter responsible for the interface stabilization. The highest interfacial adhesion can be expected to result from a combination of sufficient chain space, mobility, and length. At lower grafting densities the IFSS decreases, because the low number of entangled chains is insufficient to strengthen the fiber−matrix interface. At low IFSS, the tethered polymers even reduce the interfacial adhesion, which corresponds to a lubricating effect. In conclusion, the general expectation that long polymer chains at the surface always stabilize the composition is not valid.

To summarize, the influence of the grafting density on the interfacial adhesion is illustrated in Figure 9: Maximum IFSS is expected for a strong penetration of the buoy chains into the matrix, combined with a large number density of buoy chains. Both an increase and decrease of grafting density (of buoy chains) can result in a lowering of IFSS. This is due to two different mechanisms: A further increase of grafting density will result in a poor intermixing of matrix and polymeric coating, which is related to autophobic dewetting (see Figure 9, left).[52−54] A reduction of grafting density on the other hand will diminish IFSS as well, because it lowers the interaction energy, which is proportional to the number density of available buoy chains (see Figure 9, right).

4. CONCLUSION

The influence of different polymeric fiber coatings on the interfacial shear strength of epoxy resin based composite materials has been studied. Utilizing thiol−ene photochemistry, we introduced polystyrene chains of variable length and chain density to sulfhydrylated glasslike surfaces and characterized their morphology. "Grafting-onto" of preformed diblock copolymer from a nonselective solvent resulted in buoy-anchor arrangements of densely packed polymer coils (low density, $\sigma <$ 0.1 chains/nm^2). As a complementary method, we applied "grafting-from" polymerization generating closed films of brush-like homopolymer with coating thickness up to 225 nm.

"Grafting-onto" modified samples exhibited higher IFSS compared to "grafting-from" films. Interestingly, for both approaches a trend of higher IFSS for lower grafting densities could be identified. High chain density results in reduced IFSS and counteracts interfacial adhesion (lubrication effect) due to an inhibited penetration of polymer chains into the matrix (energetically unfavorable stretching of the chains inside of the brush-film).

Effective adhesion promotion is realized by lower chain density, since the adhesion mechanism relies on the mixing of grafted polymer and matrix material (interphase formation). Basically the interplay between enthalpic and entropic effects in the interphase determines the stability of the composition at the nanoscopic and microscopic level.We suppose that entropic effects play a significant role in interfacial interactions of coating-matrix systems. Thus interfacial adhesion in composites can be promoted, even if the constituent materials are of moderate compatibility.

This is significant for all applications where constituent components need to be combined. High adhesion between matrix and dispersed phase allows for improved transfer of load and stress. This especially holds true for fiber-reinforced composites, where the load is primarily carried by the dispersed fibers and the matrix is serving as a binding support. The formation of an interphase, a mixed phase of surface tethered chains and the embedding medium, may provide further stabilization of the composition. To attain high interfacial adhesion, strong interactions between the two materials are a prerequisite. Apart from covalent attachment, the application of polymeric interphases in the vicinity of the fiber−matrix interface embodies a versatile tool to further improve and develop advanced composite materials.

On the basis of these findings, optimization of chain density rather than maximization has to be considered in synthetic strategies for fiber-reinforced composite formation. As we clearly demonstrated, lower surface densities can lead to an increase of IFSS, which is counterintuitive, but in-line with expectations of polymer physics. As well, we introduced in this work UV-initiated thiol−ene photochemistry as an upscalable approach, which allows us to consider this important industrial parameter.

Further studies should focus on the quantification of the interaction mechanism of polymer and resinous matrix, and their mixing in the molecular gradient phase. The regime of ideal grafting density is system specific and could be quantified using substrates with grafting density gradients.[34,35]

■ ASSOCIATED CONTENT

Ⓢ Supporting Information

Size exclusion chromatography; ^{1}H NMR spectroscopy; evaluation of film thickness by AFM; single fiber pull-out test. This material is available free of charge via the Internet at http://pubs.acs.org/.

■ AUTHOR INFORMATION

Corresponding Author

*E-mail: andreas.fery@uni-bayreuth.de.

Author Contributions

All authors have given approval to the final version of the manuscript.

Funding

Financial support was given by the German Federal Ministry of Education and Research (BMBF) in the framework of a "Bionic Initiative" (0313765 A,D).

Notes

The authors declare no competing financial interest.

■ ACKNOWLEDGMENTS

The authors appreciate fruitful discussions with Annabelle Bertin (BAM Berlin), Melanie Pretzl, Christoph Hanske, Johann Erath, and Wolfgang Häfner (University of Bayreuth). They are also thankful to Ute Kuhn (University of Bayreuth) for help with TGA measurements, Martina Heider (BIMF) for help with electron microscopy, and Susann Weichold (MPI Golm) for help with the pull-out tests. We are also grateful to John Dunlop for proofreading of the manuscript.

■ REFERENCES

(1) Brondsted, P.; Lilholt, H.; Lystrup, A. *Annu. Rev. Mater. Res.* **2005**, *35*, 505−538.

(2) Corum, J.; Battiste, R.; Ruggles, M.; Ren, W. *Compos. Sci. Technol.* **2001**, *61*, 1083−1095.

(3) Sun, L.; Gibson, R. F.; Gordaninejad, F.; Suhr, J. *Compos. Sci. Technol.* **2009**, *69*, 2392−2409.

(4) Zhang, C.; Hankett, J.; Chen, Z. *ACS Appl. Mater. Interfaces* **2012**, *4*, 3730−3737.

(5) Duchet, J.; Chapel, J.-P.; Chabert, B.; Gerard, J.-F. *Macromolecules* **1998**, *31*, 8264−8272.
(6) Drown, E.; Almoussawi, H.; Drazal, L. *J. Adhes. Sci. Technol.* **1991**, *5*, 865−881.
(7) Awaja, F.; Gilbert, M.; Kelly, G.; Fox, B.; Pigram, P. J. *Prog. Polym. Sci.* **2009**, *34*, 948−968.
(8) Dunlop, J. W. C.; Weinkamer, R.; Fratzl, P. *Mater. Today* **2011**, *14*, 70−78.
(9) Fratzl, P.; Weinkamer, R. *Prog. Mater. Sci.* **2007**, *52*, 1263−1334.
(10) Gröschel, A. H.; Löbling, T. I.; Petrov, P. D.; Müllner, M.; Kuttner, C.; Wieberger, F.; Müller, A. H. E. *Angew. Chem., Int. Ed.* **2013**, *52*, 3602−3606.
(11) Geckeler, K. E.; Rupp, F.; Geis-Gerstorfer, J. *Adv. Mater.* **1997**, *9*, 513−518.
(12) Olmos, D.; Bagdi, K.; Mozco, J.; Pukanszky, B.; Gonzalez-Benito, J. *J. Colloid Interfaces Sci.* **2011**, *360*, 289−299.
(13) Iglesias, J. G.; Gonzalez-Benito, J.; Aznar, A. J.; Bravo, J.; Baselga, J. *J. Colloid Interface Sci.* **2002**, *250*, 251−260.
(14) Gao, X.; Jensen, R. E.; McKnight, S. H.; Gillespie, J. W. *Composites, Part A* **2011**, *42*, 1738−1747.
(15) Gao, S.; Mader, E. *Composites, Part A* **2002**, *33*, 559−576.
(16) Kuttner, C.; Tebbe, M.; Schlaad, H.; Burgert, I.; Fery, A. *ACS Appl. Mater. Interfaces* **2012**, *4*, 3485−3492.
(17) Gu, Y.; Li, M.; Wang, J.; Zhang, Z. *Carbon* **2010**, *48*, 3229−3235.
(18) Ciprari, D.; Jacob, K.; Tannenbaum, R. *Macromolecules* **2006**, *39*, 6565−6573.
(19) Shen, T.; Zhou, X.; Lin, Q. *Compos. Interfaces* **2011**, *18*, 701−714.
(20) Minko, S. In *Polymer Surfaces and Interfaces*, 1st ed.; Stamm, M., Ed.; Springer: Berlin, 2008; Chapter 11, pp 215−234.
(21) Pisanova, E.; Zhandarov, S.; Mader, E. *Composites, Part A* **2001**, *32*, 425−434.
(22) Miller, B.; Muri, P.; Rebenfeld, L. *Compos. Sci. Technol.* **1987**, *28*, 17−32.
(23) Schacher, F.; Yuan, J.; Schoberth, H. G.; Müller, A. H. E. *Polymer* **2010**, *51*, 2021−2032.
(24) Kern, W.; Puotinen, D. A. *RCA Rev.* **1970**, *31*, 187−206.
(25) Bywater, S.; Firat, Y.; Black, P. E. *J. Polym. Sci. Polym. Chem.* **1984**, *22*, 669−672.
(26) Marques, C. M.; Joanny, J. F. *Macromolecules* **1989**, *22*, 1454−1458.
(27) Bertin, A.; Schlaad, H. *Chem. Mater.* **2009**, *21*, 5698−5700.
(28) Chen, J.-J.; Struk, K. N.; Brennan, A. B. *Langmuir* **2011**, *27*, 13754−13761.
(29) Hoyle, C. E.; Bowman, C. N. *Angew. Chem., Int. Ed.* **2010**, *49*, 1540−1573.
(30) Löbbicke, R.; Chanana, M.; Schlaad, H.; Pilz-Allen, C.; Günter, C.; Möhwald, H.; Taubert, A. *Biomacromolecules* **2011**, *12*, 3753−3760.
(31) Tsukruk, V. V.; Singamaneni, S. *Scanning Probe Microscopy of Soft Matter: Fundamentals and Practices*, 1st ed.; Wiley-VCH: Weinheim, Germany, 2012, Ch. 3−5, 35−151.
(32) Binnig, G.; Quate, C.; Gerber, C. *Phys. Rev. Lett.* **1986**, *56*, 930−933.
(33) Gan, Y. *Surf. Sci. Rep.* **2009**, *64*, 99−121.
(34) Genzer, J.; Bhat, R. R. *Langmuir* **2008**, *24*, 2294−2317.
(35) Luzinov, I.; Minko, S.; Tsukruk, V. V. *Soft Matter* **2008**, *4*, 714−725.
(36) Liu, Y.; Klep, V.; Zdyrko, B.; Luzinov, I. *Langmuir* **2005**, *21*, 11806−11813.
(37) Ionov, L.; Zdyrko, B.; Sidorenko, A.; Minko, S.; Klep, V.; Luzinov, I.; Stamm, M. *Macromol. Rapid Commun.* **2004**, *25*, 360−365.
(38) Stuart, M. A. C.; Huck, W. T. S.; Genzer, J.; Müller, M.; Ober, C.; Stamm, M.; Sukhorukov, G. B.; Szleifer, I.; Tsukruk, V. V.; Urban, M.; Winnik, F.; Zauscher, S.; Luzinov, I.; Minko, S. *Nat. Mater.* **2010**, *9*, 101−113.
(39) Luzinov, I.; Minko, S.; Tsukruk, V. V. *Prog. Polym. Sci.* **2004**, *29*, 635−698.
(40) Arifuzzaman, S.; Oezcam, A. E.; Efimenko, K.; Fischer, D. A.; Genzer, J. *Biointerphases* **2009**, *4*, FA33−FA44.
(41) Zdyrko, B.; Luzinov, I. *Macromol. Rapid Commun.* **2011**, *32*, 859−869.
(42) Zdyrko, B.; Swaminatha Iyer, K.; Luzinov, I. *Polymer* **2006**, *47*, 272−279.
(43) Barbey, R.; Lavanant, L.; Paripovic, D.; Schüwer, N.; Sugnaux, C.; Tugulu, S.; Klok, H.-A. *Chem. Rev.* **2009**, *109*, 5437−5527.
(44) Zhao, J.; Chen, M.; An, Y.; Liu, J.; Yan, F. *Appl. Surf. Sci.* **2008**, *255*, 2295−2302.
(45) Klep, V.; Minko, S.; Luzinov, I. *PMSE Prepr.* **2003**, *89*, 248−249.
(46) Luzinov, I.; Julthongpiput, D.; Liebmann-Vinson, A.; Cregger, T.; Foster, M. D.; Tsukruk, V. V. *Langmuir* **2000**, *16*, 504−516.
(47) Cramer, N. B.; Reddy, S. K.; Cole, M.; Hoyle, C.; Bowman, C. N. *J. Polym. Sci. Polym. Chem.* **2004**, *42*, 5817−5826.
(48) Yoon, D. Y.; Sundararajan, P. R.; Flory, P. J. *Macromolecules* **1975**, *8*, 776−783.
(49) Kim, B.; Yeol, Ryu; Du; Pryamitsyn, V.; Ganesan, V. *Macromolecules* **2009**, *42*, 7919−7923.
(50) Brittain, W. J.; Minko, S. *J. Polym. Sci. Polym. Chem.* **2007**, *45*, 3505−3512.
(51) Qian, L. L.; Bruce, F. A.; Kellar, J. J.; Winter, R. M. *Meas. Sci. Technol.* **1995**, *6*, 1009−1015.
(52) Jopp, J.; Yerushalmi-Rozen, R. *Macromolecules* **1999**, *32*, 7269−7275.
(53) Reiter, G.; Khanna, R. *Langmuir* **2000**, *16*, 6351−6357.
(54) Beziel, W.; Reiter, G.; Drockenmuller, E.; Ostaci, R. V.; Akhrass, Al, S.; Cousin, F.; Sferrazza, M. *EPL* **2010**, *90*, 26008p1−p6.
(55) Gutowski, W.; Li, S.; Russell, L.; Filippou, C.; Hoobin, P.; Petinakis, S. *Compos. Interfaces* **2002**, *9*, 89−133.
(56) Gutowski, W. *J. Adhes.* **2003**, *79*, 445−482.
(57) Gutowski, W.; Li, S.; Filippou, C.; Hoobin, P.; Petinakis, S. *J. Adhes.* **2003**, *79*, 483−519.